(6) Moscowitz, A. *Adv. Chem. Phys.* **1962**, *4*, 67-112.
(7) Djerassi, C. *Optical Rotatory Dispersion*; McGraw-Hill: New York, 1960.
(8) Stephens, P. J. *Annu. Rev. Phys. Chem.* **1974**, *25*, 201-232.
(9) Djerassi, C.; Bunnenberg, E.; Elder, D. L. *Pure Appl. Chem.* **1971**, *25*, 57-90.
(10) Shashova, V. E. *J. Am. Chem. Soc.* **1960**, *82*, 5505-5506.
(11) Pidgeon, C. R.; Smith, S. D. *Infrared Phys.* **1964**, *4*, 13-28.
(12) Bloembergen, N.; Shen, Y. R. *J. Opt. Soc. Am.* **1964**, *54*, 551-552.
(13) Church, D. A.; Hadeishi, T. *Appl. Phys. Lett.* **1973**, *24*, 185-187.
(14) Ito., M.; Murayama, K.; Kayama, K.; Yamamoto, M. *Spectrochim. Acta, Part B* **1977**, *32B*, 347-355.
(15) Kitagawa, K.; Shigeyasu, T.; Takeuchi, T. *Analyst* **1978**, *103*, 1021-1030.
(16) Kersey, A. D.; Dawson, J. B. *Anal. Proc. (London)* **1981**, *18*, 187-189.
(17) Debus, H.; Hanle, W.; Scharmann, A.; Witz, P. *Spectrochim. Acta, Part B* **1981**, *36B*, 1015-1021.
(18) Yamamoto, M.; Murayama, S.; Ito, M.; Yasuda, M. *Spectrochim. Acta, Part B* **1980**, *35B*, 43-50.
(19) Kawazumi, H.; Nishimura, H.; Ogawa, T. *Anal. Sci.* **1990**, *6*, 135-136.
(20) Partington, J. R. *Advanced Treatise on Physical Chemistry*; Longmans, Green & Co.: London, 1954; p 602.
(21) Hougen, J. T. *J. Chem. Phys.* **1960**, *32*, 1122-1125.
(22) Waring, C. E.; Hyman, H.; Steingiser, S. *J. Am. Chem. Soc.* **1940**, *62*, 2028-2031.
(23) Broersma, S.; Waterman, H. I.; Westerdijk, J. B.; Wiersma, E. C. *Physica* **1943**, *10*, 97-129.
(24) Washburn, E. W. *International Critical Tables*; McGraw-Hill: New York, 1926; Vol. VI, p. 425.
(25) Schrönrock, V. O. *Z. Phys.* **1932**, *78*, 707-721.
(26) Chuckerbutti, B. N. *Indian J. Phys.* **1932**, *8*, 387-395.
(27) Yeung, E. S., Steenhoek, L. E.; Woodruff, S. D.; Kuo, J. C. *Anal. Chem.* **1980**, *52*, 1399-1402.
(28) Xi, X.; Yeung, E. S. *Appl. Spectrosc.* **1989**, *43*, 1337-1341.
(29) Montgomery, D. B. In *Solenoid Magnet Design*; Krieger, R. E., Ed.; R. E. K. Publishing Co.: Huntington, NY, 1980; p 6.
(30) Bobbitt, D. R.; Yeung, E. S. *Appl. Spectrosc.* **1986**, *40*, 407-409.
(31) Monnig, C. A.; Madison, R. T.; Heiftje, G. M. *Appl. Spectrosc.* **1990**, *44*, 216-219.
(32) Monnig, C. A.; Heiftje, G. M. *J. Anal. At. Spectrosc.* **1988**, *3*, 679-682.
(33) Oldenbourg, R.; Phillips, W. C. *Rev. Sci. Instrum.* **1986**, *57*, 2362-2365.
(34) Yeung, E. S. *Talanta* **1985**, *32*, 1097-1100.
(35) Stephen, M. J. *Mol. Phys.* **1958**, *1*, 301-304.
(36) Partington, J. R. *Advanced Treatise on Physical Chemistry*; Longmans, Green & Co.: London, 1954; p 607.
(37) Foehr, E. G.; Fenske, M. R. *Ind. Eng. Chem.* **1949**, *41*, 1956-1966.
(38) Dovichi, N. J.; Harris, J. M. *Anal. Chem.* **1979**, *51*, 728-731.
(39) Woodruff, S. D.; Yeung, E. S. *Anal. Chem.* **1982**, *54*, 2124-2125.
(40) Forsythe, J. G.; Kieselbach, R.; Shashoua, V. E. *Appl. Phys.* **1967**, *6*, 699-702.

RECEIVED for review September 4, 1990. Accepted November 30, 1990. The Ames Laboratory is operated by Iowa State University for the U.S. Department of Energy under Contract W-7405-Eng-82. This work was supported by the Director of Energy Research, Office of Basic Energy Sciences, Division of Chemical Sciences.

Fluorescence Detection in Capillary Zone Electrophoresis Using a Charge-Coupled Device with Time-Delayed Integration

J. V. Sweedler, J. B. Shear, H. A. Fishman, and R. N. Zare*

Department of Chemistry, Stanford University, Stanford, California 94305

R. H. Scheller

Howard Hughes Medical Institute, Department of Molecular and Cellular Physiology, Stanford University, Stanford, California 94305

A fluorescence detection system for capillary zone electrophoresis is described in which a charged-coupled device (CCD) views a 2-cm section of an axially illuminated capillary column. The CCD is operated in two readout modes: a snapshot mode that acquires a series of images in wavelength and capillary position, and a time-delayed integration mode that allows long exposure times of the moving analyte zones. By use of the latter mode, the ability to differentiate a species based on both its fluorescence emission and migration rate is demonstrated for fluorescein and sulforhodamine 101. The detection limit for fluorescein isothiocyanate (FITC) is 1.2 × 10^{-20} mol; detection limits for FITC-amino acids are in the (2-8) × 10^{-20} mol range.

INTRODUCTION

Numerous research areas in biochemistry depend on the ability to analyze minute quantities of nucleic acids, amino acids, and peptides, yet many present detection schemes have inadequate sensitivity. Examples are the analyses of single cells and subcellular compartments. One of the few techniques to permit successful assays of the contents of a single cell (*1-4*) is capillary zone electrophoresis (CZE), a powerful separation technique for the analysis of small sample volumes. Separation efficiencies routinely exceed several hundred thousand theoretical plates, and typical injection volumes are 10 nL or less. Several recent reviews describe the capabilities and performance of CZE in detail (*5-9*).

For CZE, channel diameters usually range from 25 to 100 μm; therefore, designing methods to detect low concentrations in these small-diameter capillaries is a challenge. Laser-induced fluorescence (LIF) is currently the most sensitive detection method for CZE; detection limits are in the low attomole range (*10-12*). In these systems, the capillary is used as the "flow cell", the laser illumination is perpendicular to the capillary, and a photomultiplier tube (PMT) monitors the fluorescence. Dovichi and co-workers (*13-15*) developed a more sensitive method that has the same excitation geometry but uses a sheath flow cuvette as the sample cell and thereby eliminates much of the scattered light and luminescence from the fused silica capillary. With this technique, detection limits in the low zeptomole range for fluorescently tagged amino acids have been reported. [Zepto (z) and yocto (y) have been proposed as the new SI prefixes for 10^{-21} and 10^{-24}, respectively, by the Comité Consultatif des Unités; final approval is pending the next meeting of the Comité Général des Poids et Mesures.]

The LIF/CZE system described here uses a two-dimensional charge-coupled device (CCD) containing an array of 516

0003-2700/91/0363-0496$02.50/0

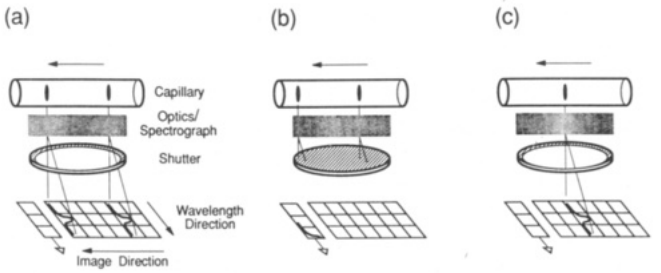

Figure 1. Diagram of the CCD/LIF system illustrating the snapshot mode. (a) The shutter is opened to expose the CCD to the fluorescence of two analyte bands. (b) After exposure, the shutter is closed and the photogenerated charge information is read. (c) When the shutter next opens, the analyte bands have traveled along the capillary, and one band remains in the observation zone.

by 516 detector elements. Several reviews describe the advantages and operating characteristics of CCDs for fluorescence work (*16–19*). Although CCDs can have a lower dark current and higher quantum efficiency than the best PMTs, they suffer from a small but significant readout noise. An important advantage of CCDs is their two-dimensional format; CCDs are available in arrays ranging from 64 by 64 to more than 2048 by 2048 elements. To date, several reports have described optical array detectors employed with CZE, including the use of a photodiode array as a multichannel UV–vis absorbance detector (*20, 21*) and a CCD as a multichannel fluorescence detector (*22*).

We present a unique axial illumination arrangement for CZE that has several advantages when used with multichannel detectors. The output of a laser is focused into the end of the capillary, the fluorescence emission from the analyte is collected over a 2-cm section of the channel, and the entire fluorescence spectrum is measured by using the CCD array. In this way, the fluorescence cell is on-column, and the complete fluorescence spectrum is acquired simultaneously. Residence times for analytes in the 2-cm observation zone range from 2 to 45 s. The axial illumination method allows the CCD to be operated in two readout modes and provides significant advantages over conventional illumination and CCD detection. These readout modes, the *snapshot mode* and the *time-delayed integration* (TDI) *mode*, are described below.

Snapshot Mode. Although the large format of many CCDs offers considerable flexibility to the researcher, their slow readout rate is often a drawback. Most scientific CCDs have a readout rate of 50 kHz/element, requiring several seconds to read out a large array. Consequently, CCDs are used primarily with shutters to take sequences of snapshots (*19*). After exposure of the detector to the fluorescence signal, the shutter is closed and the photogenerated charge information is digitized. The long delays between subsequent exposures limit the usefulness of this readout mode in acquiring information from a changing scene, such as occurs in CZE.

In the one published report on CZE with a CCD, more than 5 s was required to read the CCD and transfer the data to the host computer after each 0.2-s exposure (*22*). In CZE, peak widths typically range from 0.5 to 5 s; thus, an entire analyte band can be missed because the shutter is closed during the time the band is in the observation zone. Even if some of the sample is observed, quantitation becomes problematic because the exposure time of the analyte to the CCD is not known.

Axial illumination eliminates the problems of missing bands and incomplete analyte exposures. Figure 1 illustrates the snapshot mode for an axially illuminated capillary by using a simplified 3 by 6 element CCD. Although the analyte bands migrate during the period that the shutter is closed, the second band is still in the observation zone during the next exposure. The choice of a 2-cm observation zone means that at least 1

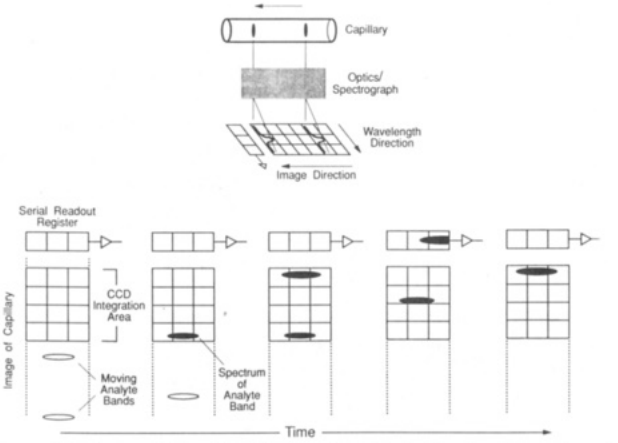

Figure 2. Digram of the CCD/LIF system illustrating the time-delayed integration (TDI) mode. The CCD is oriented so that the parallel shift direction is the same as the analyte band motion. As the emission of the analyte bands moves across the CCD, the CCD shifts the resultant photogenerated charge information at the same rate. When the photogenerated charge from each band reaches the serial readout register, the spectrum is read and digitized.

but usually from 10 to 30 complete exposures of every analyte are obtained. In addition, the snapshot mode is useful for optical system diagnostics, as it allows tracking of individual bands and real-time feedback for focusing the optics.

The low duty cycle of the detector (i.e., most of the time the shutter is closed) is far from ideal. Moreover, the use of a CCD to take a series of snapshots creates the need to extract information from multiple exposures. With CCDs, the problems with data accumulation are severe. For a 516 by 516 element CCD, such as the one employed in our work, each complete CCD read generates 0.5 Mbytes of data. If, for example, the CCD is read every 3 s, nearly 300 Mbytes of data per CZE run is generated; extracting the fluorescence intensity from this information is not trivial.

Time-Delayed Integration Mode. The TDI readout mode was developed for satellite surveillance work when a CCD has a limited time to integrate the signal from a fixed point on the ground as a satellite passes overhead (*23*). It is also ideally suited to LIF/CZE with axial illumination, in which the analyte band passes through an extended detection zone. By use of this technique, the CCD becomes a highly sensitive and flexible multichannel fluorescence detection system. TDI does not use a shutter, can acquire an entire spectrum in 50 ms, and can spatially resolve multiple bands that are in the observation zone. Furthermore, far less data are generated than in the snapshot mode.

To understand the TDI technique, a brief description of CCD operation is necessary. In a CCD, all the photogenerated charge in the photoactive elements is transferred toward the serial register one row at a time, and the charge information in the serial row is read by using the single on-chip amplifier (*16*). For a 516 by 516 element CCD, each time a single imaging area is transferred to the serial register, 516 readouts are performed; each readout corresponds to a different spectral element. This process continues until all 516 rows have been read 516 times.

Normally these transfers are done with the shutter closed to prevent exposure of the CCD to the illumination source; if such exposure occurs, the image becomes blurred. In our work, we eliminate the shutter and synchronize the shifting of rows to the migration rate of the analyte band in our capillary. Figure 2 illustrates the TDI mode by using a simplified 3 by 4 element CCD and two analyte bands. As an analyte band enters the laser excitation zone, the fluorescence is collected and illuminates the first row of the CCD. From here, the band takes a period of time to migrate to the point on the

capillary from which its image is projected onto the CCD one row closer to the serial register. After this time, the charge in the CCD is shifted toward the serial register by one row so that the analyte fluorescence signal still contributes to the same charge information. It is important to distinguish between the physical rows of the CCD and the continually moving row of accumulating photogenerated charge. The effective integration time for a given analyte band is the entire time the band is in the observation zone; however, multiple bands can be within this zone simultaneously and still be resolved because of their different spatial positions.

The TDI mode has several important advantages. Only one row of the CCD is read at a time, reducing the data produced and the readout time up to 516-fold (depending on the spatial binning factor). Also, a row contains the fluorescence from a single analyte and not from a point on the capillary; the fluorescence is integrated over the entire time the band is in the observation zone. A third advantage is that the fluorescence information from the analyte band can be obtained from a single CCD readout instead of the approximately 4–20 readouts required with the snapshot mode. The single readout produces a 2- to 5-fold reduction in read noise.

In CZE, the TDI mode is complicated by the fact that the analyte bands move at different rates because of their different electrophoretic mobilities. Hence, the shift rate must be continually decreased during the run to follow different bands. The synchronization of the shift rate to the analyte velocity needs to be accurate to avoid a loss in separation efficiency. Fortunately, such synchronization is not difficult to obtain. Because both the start time of the CZE run and the distance from the injector to the center of the observation zone are known, the shift time can be determined by

$$T_{shift} = (T_{elapsed} X_{obs} N_{bin}) / (N_{ccd} L_{cap}) \quad (1)$$

where T_{shift} is the time until the next CCD shift, $T_{elapsed}$ is the time since the start of the CZE run, X_{obs} is the length of the observation zone, N_{bin} is the binning factor in the observation (imaging) dimension, N_{ccd} is the number of CCD elements the capillary image illuminates, and L_{cap} is the length of the capillary to the center of the observation zone. The integration times range from 2 to 45 s for a 80-cm capillary, 2-cm observation zone, and analyte elution times from 1 to 30 min.

A CCD must shift charge from all rows in concert (i.e., the shift rate is the same for all rows). Because each row receives a signal that originates from a different point in the capillary, the shift rate must be *incorrect* for all but one specified row. To visualize this concept, consider two analyte bands that are resolved and are in the detection region simultaneously. They must be moving at slightly different velocities because they are resolved; the CCD, which shifts at a single velocity, cannot independently track both. In these experiments, in which we have matched the shift rate to the center of the 2-cm observation zone at the end of an 80-cm capillary, a ±1% difference between the zone velocity at the observation boundaries and TDI shift rate is expected. Thus, in the configuration we employ, almost no increase in analyte zone width is expected.

Immediately after injection, the required time between shifts is less than 50 ms. Because the system cannot shift this fast, the tracking of this extremely fast moving (hypothetical) band is not exact. Currently, the system shifts at the maximum rate until the calculated shift rate is slower than 20 Hz (for approximately 2 min), at which point it shifts at the appropriate rate. Because the shift rate is always decreasing, data are obtained with a nonuniform time resolution, although the spatial resolution remains constant (the system images every band with the same 80-μm resolution). Thus, the early fast bands are sampled faster than later bands. This type of sampling scheme fits well with constant resolution and data acquisition per band (*24*).

A simple method exists to preclude the need for a changing shift rate and thus to avoid the potential blurring caused by the TDI method. If the capillary is grounded just prior to the observation zone (*25*, *26*), the analyte bands would not undergo electrophoresis while being detected and instead would move at the solution flow velocity. Because the separation efficiency obtained with the present method is sufficient for a wide range of applications, these experiments have not yet been undertaken.

Using the TDI mode, we can obtain CZE electropherograms with over 700 000 theoretical plates. In addition, we obtain sensitivities for fluorescent tags in the low zeptomole range and can differentiate between multiple fluorophores based on different migration times and spectral characteristics.

EXPERIMENTAL SECTION

Axial Illumination. To achieve high sensitivity with the CCD system using either of these CCD readout modes, longer exposure of the CCD to the analyte fluorescence is advantageous. In most LIF/CZE systems, the laser beam diameter is focused to less than 50 μm and strikes the capillary perpendicular to the separation channel; thus, the analyte is illuminated by the laser for only several milliseconds. In the system described here, the capillary is illuminated end-on, and the resultant fluorescence from a 2-cm section is imaged onto the CCD. Fluorescence is collected during the entire residence time of the analyte band in this section.

Problems could occur when axially illuminating a capillary that contains a leading band at high concentration closely followed by other bands. The leading band could absorb a significant fraction of the channeled excitation light, thus reducing the fluorescent signal from later bands also resident in the observation zone. However, we do not observe such a shadowing effect at the fluorophore concentrations used in this work.

A buffer-filled capillary does not fulfill the requirements of a light pipe; the index of refraction of the aqueous center is lower than that of the fused silica "cladding". Thus, laser illumination tends to travel in the fused silica wall rather than propagate through the center of the capillary, unless care is taken in the choice of laser-focusing lens and the alignment of the laser beam with respect to the capillary. The focusing lens is chosen to prove a beam waist just smaller than the capillary inside diameter. This lens provides a large depth of field and hence an extended illumination zone. Even with these measures, illumination travels only several centimeters in the capillary channel before significant attenuation occurs.

An axially illuminated open tubular liquid chromatography (OTLC) system has been described using capillaries of similar dimensions, but in that case, the solvent was chosen to provide a higher index than the quartz capillary material (*27*). For axial illumination of the OTLC system, the laser beam must be propagated through the length of the capillary. In our case, however, the loss of light after several centimeters is desirable. Many fluorophores, including fluorescein, photodegrade rapidly under moderate-intensity illumination; thus, illumination of the analyte band prior to the detection zone is deleterious. For a water-filled fused silica capillary, light radiates from the aqueous channel into the walls as the capillary bends (*27*, *28*). Thus, the channel is bent sharply (90° bend over 1 cm) before the 2-cm observation zone. This bending prevents laser light from propagating much past the observation zone and thus greatly reduces photodegradation of the fluorophore before detection. Additionally, the bend in the capillary prevents ambient room light from propagating through the capillary to the detection region.

In conventional systems, when the laser power is high, photodegradation occurs but the fluorescence of the fluorophores is still monitored. In our system, a 1-cm distance separates the bend in the capillary and the beginning of the observation zone. Thus, for 1 cm, or up to 20 s, the fluorescently tagged analyte is subject to laser illumination without collection of the resultant fluorescence. To limit premature photodegradation and a consequent reduction in sensitivity, laser power must be extremely low. Currently, we are developing an improved capillary holder that will sharply reduce this *dead zone* distance. The low-intensity illumination and the long observation time are expected to provide the highest signal-to-noise ratios obtainable from a fluorophore

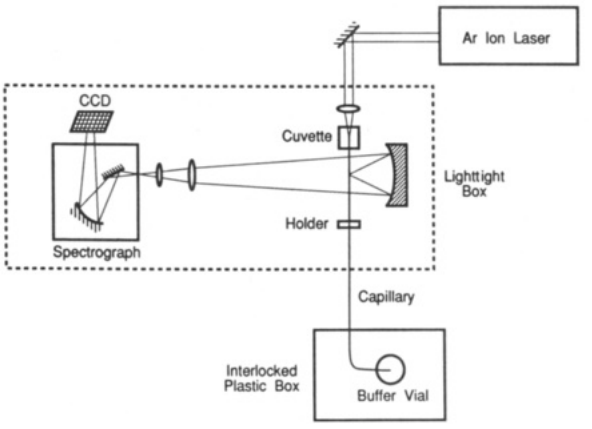

Figure 3. Schematic diagram showing the Ar ion laser, capillary arrangement, optics, and CCD detector.

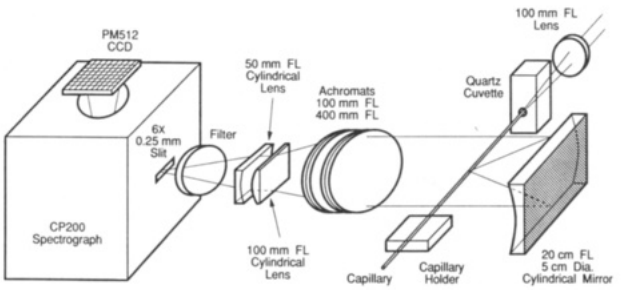

Figure 4. Detailed schematic of the optical system from Figure 3, showing the axially illuminated capillary. The optics form a 250-μm by 6-mm image of a 63-μm by 2-cm section of capillary on the entrance slit of the spectrograph.

susceptible to photodegradation (*29*).

An argon-ion laser (Model 164, Spectra-Physics, Mountain View, CA) provides the laser illumination, and a 488-nm or 514-nm laser-line interference filter (Oriel Corporation, Stratford, CT) blocks all but the desired wavelength. For most studies, the laser is operated on the lowest power light-stabilized mode (100 mW), and several neutral density filters are used to reduce the power illuminating the capillary to between 35 and 175 μW. These illumination levels may be the lowest reported for LIF detection. For all studies except the multiple fluorophore experiment, 488 nm is employed. A 100-mm focal length (fl) fused silica lens (LQP007, Melles Griot, Irvine, CA) is used to focus the laser into the 63-μm-i.d. capillary. The capillary alignment is controlled by two linear translation stages and a two-axis tilt stage (Newport Research Corp., Irvine, CA) to allow precise alignment with the laser beam.

Detection System. The overall detection system is shown in Figure 3, and a more detailed view of the optical system appears in Figure 4. As shown in Figure 3, the optics form an image of the capillary on the CCD, and a spectrograph disperses the image. Hence, the two dimensions of the CCD array contain different information; one contains the image of the capillary and the other contains wavelength information. For clarity, we define rows as the dispersive dimension and columns as the capillary image dimension. Thus, the fluorescence from one spot on the capillary (or one analyte band at a particular time) is dispersed along a row of the array. Because the requirements for the optics are different in the two dimensions, cylindrical optics are used.

The optical system consists of five elements. It was designed with the aid of Beam 3 Optical Ray Tracer (Stellar Software) to maximize the light collection while minimizing aberrations. The first element is a 20-cm fl cylindrical mirror (LCP 178, Melles Griot), used instead of a lens to reduce chromatic and spherical aberrations. Next are two achromats (used as the imaging elements) and two cylindrical lenses (LAO 288, LAO126, LCP155, and LCN129, Melles Griot, respectively). To simplify the alignment of the system, the two cylindrical lenses are held in a single mount, the two achromats are in another mount, and the slit of the spectrograph is fixed. The overall system is designed to form an image of a 2.5-cm by 50-μm capillary on the 6- by 0.25-mm slit of the spectrograph. This system is $F/1$ in the wavelength dimension and $F/12$ in the imaging dimension; both are matched to the $F/3$ of the spectrograph.

An aberration-corrected imaging spectrograph (CP200, Instruments SA, Edison, NJ) is used because it maintains a point-to-point relation between the image of the slit and the CCD focal plane (*30*, *31*). By use of the CP200 equipped with a 133 grooves/mm grating, the field of view of the CCD is 370 nm; this wavelength window is adjustable from 200 to 1000 nm. The spectral bandwidth is approximately 0.72 nm/CCD element; the resolution is 3.6 nm using a 100-μm slit and is 9 nm using a 250-μm slit.

The detection system consists of a 516 by 516 element CCD (PM512, Photometrics Ltd., Tucson, AZ), supplied with the Metachrome II overcoating to extend the wavelength range; the quantum efficiency is more than 10% from 200 to 900 nm, with a maximum of more than 50% at 700 nm. The CCD is controlled with CCD electronics and signal-processing modules (CE200 and CC200, Photometrics Ltd.).

Characteristics that make PM512 CCD well suited to CZE include its large format, high quantum efficiency, low dark current, and low read noise. In addition, this CCD does not suffer from the charge trapping and poor charge transfer efficiency of some other scientific-grade CCDs (*32*, *33*). With the particular CCD used, the overall system readout noise can be fewer than 6 electrons; at 600 nm, this read noise corresponds to fewer than 12 photons of noise per detector element. The CCD is contained in a liquid-nitrogen-cooled cryostat to reduce the dark current. When the system is operated at −125 °C, the measured dark current is less than 2 electrons/min per detector element, an insignificant value considering the background luminescence levels found in typical "clean" solvents.

System Control. The system uses a unique set of CCD readout methods. The Photometrics CC200 camera controller is a multibus 68000 computer system with a variety of CCD operations and commands preprogrammed. Several additional commands have been added to the command library by using FORTH. The CC200 computer performs all CCD control and executes all high-level commands to the CCD detector. The CC200 computer is controlled with a high-speed IBM AT clone (System 220, Dell Computer Systems) using ASYST version 3.1 (Asyst Software Technologies, Rochester, NY) through a high-speed GPIB interface (PC2A, National Instruments, Austin, TX). Considerable effort has gone into designing computer code to optimize data acquisition and system control. The data reduction from two-dimensional spectral and spatial information to electropherogram is performed in real time by data-reduction algorithms in both computers. In addition, the Dell computer controls voltage and monitors voltage, current, and other aspects of system performance; all spectra and electropherograms are stored and displayed by using routines written in ASYST.

The CCD detector utilizes the read mode commonly referred to as *binning* (*16*, *18*). Binning is an electronic method of changing the effective detector element size, using the actual 20- by 20-μm detector elements as building blocks to make binned elements of any combination desired. Binning is accomplished by combining the photogenerated charge on-chip and then reading out the information in this combined charge packet with a single read. Because the binned information is read by using a single readout, the overall read noise is lower than in systems in which the individual detectors are read and their readouts summed in computer memory. In our system, we routinely read out the CCD in the wavelength dimension with 4-fold binning, thereby producing 128-point spectra. Because of the broad nature of molecular fluorescence spectra in solution, little information is lost when using 4-fold binning; moreover, both the amount of data generated and the effective read noise are reduced. Binning in the image dimension also reduces the amount of data generated, but in this case, spatial resolution is decreased.

As each row of the CCD is read, an entire fluorescence spectrum is acquired. For several applications, observing complete spectra is useful. For quantitative analysis, we extract the analyte intensity information by using the following method. First, a background array is subtracted from each spectrum to remove the electronic offset for each element. Next, the spectrum is multiplied by an array that contains weighting factors for each

wavelength. These weighting factors constitute a digital filter that selects the optimum wavelengths for determining the fluorescence intensity. Although sophisticated methods can be used to optimize the extraction of information, we have not yet taken such measures. For the present studies, the weighting factors are set to 1 for the wavelengths of maximum fluorescence intensity, all other weighting factors are zeroed, and the resulting intensity information is summed. For several studies, the resulting electropherograms are digitally smoothed by using Blackman's window for the convolution weights and a noise cutoff frequency of 0.33 cycles/point (*34*). This procedure reduces the higher frequency noise but has little effect on the peak width and height.

CZE Apparatus. The CZE portion of the system is similar to that described previously (*35–38*). A 4-cm section of the polyimide from the 63-μm-i.d., 363-μm-o.d. capillary (Polymicro, Phoenix, AZ) is burned off by using gentle heating in a flame. Precautions must be taken to avoid damaging the fused silica during this process. After the polyimide is removed, the end of the capillary is carefully scored and broken to leave a surface as flat as possible. Because the laser illumination is directly through the end of the capillary, any imperfections contribute greatly to scattered light. This end of the capillary is held at ground potential in a modified fluorescence quartz cuvette. The incident laser illumination is focused through the cuvette containing the buffer solution and into the capillary. The inlet end of the capillary, held at high positive voltage, is placed in a 4-mL vial containing approximately 2–3 mL of electrolyte buffer solution. The electrical circuit is completed by strips of Pt foil submersed in each buffer reservoir. All separations employ a 20-kV potential across the capillary. The current through the system is measured by monitoring the voltage drop across a 10-kΩ resistor at the ground side of the capillary. The capillary inlet is contained in an interlocked Plexiglas box, and the outlet, where detection occurs, is held in a light-tight optical enclosure.

All samples are introduced by using gravity injection in which the inlet of the capillary is removed from the buffer vial and placed in an elevated sample vial. This injection method is chosen to avoid the sampling bias associated with electrokinetic injection (*39*). For these experiments, the height displacement is 5 cm and the injection time is from 10 to 30 s, which introduces from 4 to 13 nL of sample. To prevent sample carryover from an injection, we dip the inlet into a vial of water after each injection. In addition, we have removed the polyimide from the first 5 mm of the capillary.

Reagents. The water used to prepare solutions is freshly purified (Ion-X Adsorber and Research Deionizer, Cole Parmer, Chicago, IL; LD2A Demineralizer and Mega-Pure Still, Corning Glassworks, Corning, NY). The supporting electrolyte for all the experiments is 50 mM borate (pH 9.0) prepared from reagent-grade sodium borate decahydrate and boric acid (Mallinckrodt). Stock solutions of fluorescein (Sigma), sulforhodamine 101 (Exciton), and fluorescein isothiocyanate (FITC) isomer I (Aldrich) are prepared at approximately 10^{-5} M and used without further purification. All low-concentration solutions are made daily by serial dilutions from these stock solutions. All amino acids are purchased from Sigma and used without further purification. Reagent-grade sodium bicarbonate (Sigma) and acetone (Baker) are used in the derivatization reactions described below.

Derivatization. Amino acids are derivatized with FITC isomer I in a modified version of the procedure described by Kawauchi et al. (*40*). Briefly, individual solutions of amino acids are prepared at approximately 100 mM in 200 mM $NaHCO_3$ (pH 9.0). Approximately 10 mM FITC is dissolved in a 95% acetone, 5% water solution that contains 0.001% pyridine (by volume) to catalyze the reaction. Derivatization is initiated by the addition of 100 μL of FITC solution to 500 μL of amino acid solution. The reaction is carried out in the dark at 20 °C for approximately 8 h. FITC–amino acid solutions are maintained separately in opaque vessels at 4 °C for up to 2 days and are mixed immediately prior to separation.

RESULTS AND DISCUSSION

System Performance. Figure 5 illustrates the ability of the optical system to image the capillary accurately and of the CCD/LIF system to measure the fluorescence from an analyte undergoing electrophoresis. This figure shows the focal plane output of the CCD for a single 4-nL injection of 8×10^{-10} M FITC. The CCD is used in the conventional snapshot mode, in which a shutter is placed between the capillary and the spectrograph slit to time the exposure of the CCD. After the shutter is closed, the CCD is read. Figure 5a is a 0.5-s exposure taken after approximately 13 min, 5b is taken 4 s later, and 5c, 6 s after 5b. The data in Figure 5 show the CCD output corresponding to approximately 460–600 nm, less than 50% of the spectral information stored in the CCD. To reduce the data further, the CCD is read with 4 by 4 binning, the resulting data are smoothed in the wavelength dimension, and every second wavelength point and every second spatial line are plotted. This procedure reduces the focal plane output from 250 000 detector elements to the approximately 2000 points plotted. With 4 by 4 binning, each element corresponds to an 80 by 80 μm area on the detector focal plane and a 320-μm length of capillary. Both the Rayleigh line and the strongest Raman line are clearly visible along with the fluorescence from FITC. Comparison of these images shows the motion of the FITC band.

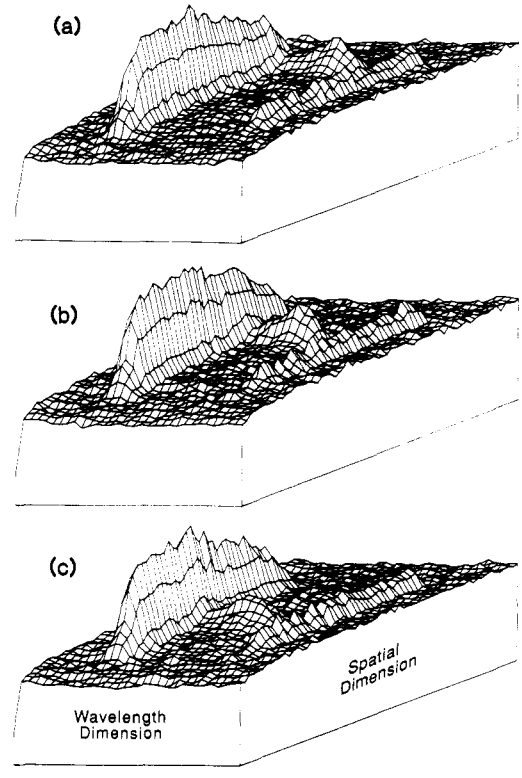

Figure 5. Snapshots (0.5-s exposures) of the focal plane output for a 4-nL injection of 8×10^{-10} M FITC: (a) taken after 13 min, (b) 4 s later, and (c) 6 s after (b). The Rayleigh and the main Raman bands of water are visible along with the moving FITC band.

Figure 6 illustrates the ability of the TDI mode to track an analyte. These electropherograms show a series of 4-nL injections of 8×10^{-10} M FITC for a variety of shift rates. In Figure 6a, the shift rate is that calculated by using eq 1; electropherograms in Figure 6b and 6c are obtained with 10% faster and 20% slower shift rates, respectively. For the optimum shift rate, the efficiency (N) is 400 000 theoretical plates, but as the shift rate is changed, N decreases; however, with a 10% error in shift rate, efficiencies of 250 000 theoretical plates are obtained. Thus, extremely accurate estimations of the shift rate are not required for most purposes.

Multiple Fluorophores. To determine the flexibility of the system to detect multiple fluorophores, we analyze a mixture of two commonly used derivitizing agents. Two changes in the detection system are made for this experiment: the laser illumination is changed to 514 nm, and a 525-nm

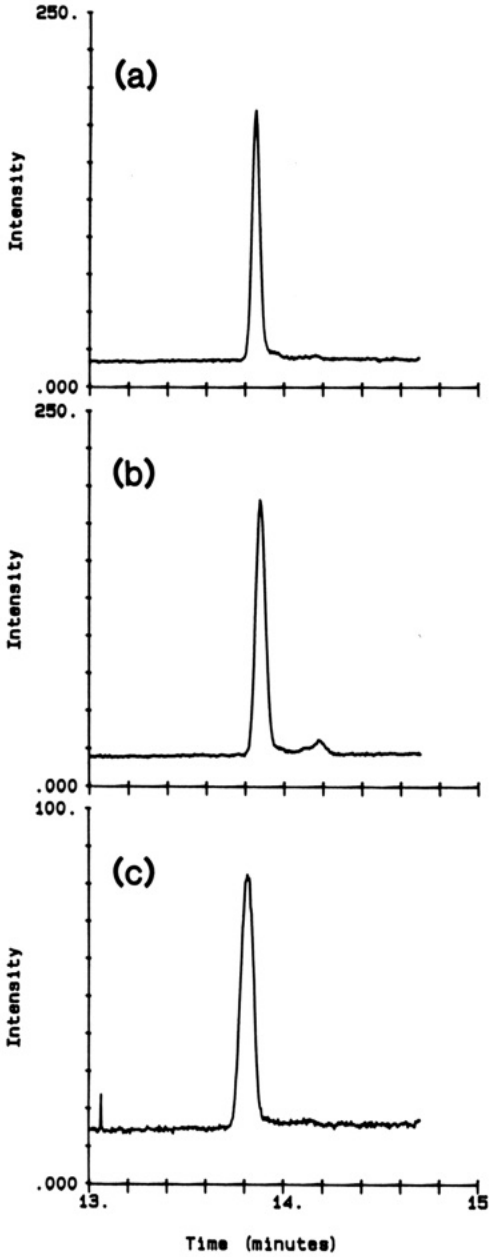

Figure 6. Electropherograms illustrating the effect of changing the TDI shift rate on electrophoretic efficiency for a series of 3-amol FITC injections. In (a), the shift rate is optimized and the efficiency (N) is 400 000. In (b), the shift rate is increased 10% and N is 250 000. In (c), the shift rate is reduced 20% from (a), and N is 150 000. The small peak to the right of the FITC peak is a contaminant.

cutoff filter is inserted before the spectrograph slit to reduce the Rayleigh scattering. Figure 7 shows the TDI electropherogram of 3×10^{-9} M sulforhodamine 101 and 9×10^{-9} M fluorescein. The CCD is binned 4-fold in the wavelength dimension, and the resulting 128-point spectra are stored. To aid visualization of the data, the CCD is read by using 16-fold binning in the image dimension, thus reducing the number of spectra from more than 25 000 to less than 2000. Every fourth spectrum collected between 9 and 14 min is plotted in Figure 7. The spectra shown in this figure are plotted with equal spacing; because of the nonlinear data-acquisition rate, the time axis is nonlinear.

Figure 7 shows the spectra of the fluorophores, as well as the 514-nm scattered light and two Raman bands from water. The fluorescence emission of the sulforhodamine is to the red of emission from fluorescein. This figure also illustrates another effect of the changing shift rate; because the data acquisition rate is continually slowing down, the background

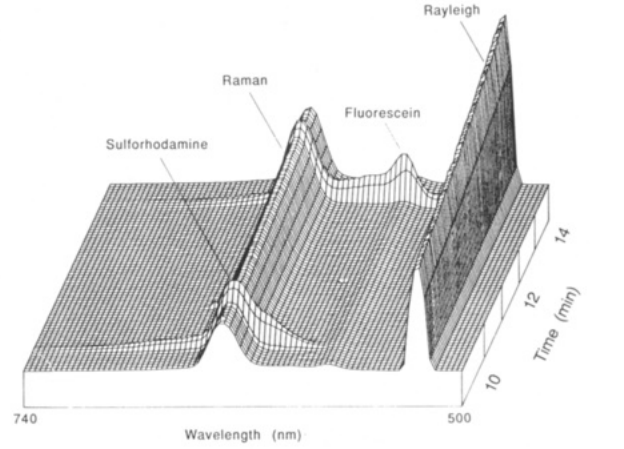

Figure 7. TDI electropherogram of sulforhodamine and fluorescein. The increase in the Raman and Rayleigh lines as the run progresses is caused by the accumulation of signal for a longer integration time for each succeeding spectrum.

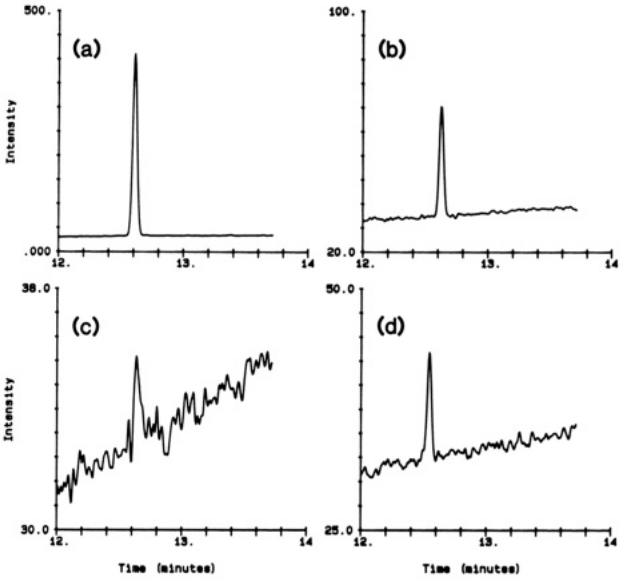

Figure 8. TDI electropherograms of FITC for the following concentrations: (a) 7×10^{-10} M, (b) 6×10^{-11} M, (c) 6×10^{-12} M, and (d) 6×10^{-12} M. The injection volume for (a), (b), and (c), is 4 nL, and for (d), 13 nL. Fluorescence intensity is obtained by using a spectral window between the Rayleigh and major Raman band. The sloping base line is caused by a continually increasing integration time corresponding to a decreasing shift rate.

(i.e., Rayleigh and Raman bands) is continually increasing in intensity. This effect does not alter the sensitivity or utility of this technique because both the analyte fluorescence and the background emission increase at the same rate with increasing integration time. If desired, however, each spectrum can be divided by its integration time. The ability to detect and differentiate multiple fluorophores is important to several applications, notably in DNA sequencing when identifying each of the four bases (*10*, *41*).

Sensitivity. Figure 8 illustrates the sensitivity of the system with a series of electropherograms of FITC. Parts a–c of Figure 8 represent 4-nL injections of 7×10^{-10}, 6×10^{-11}, and 6×10^{-12} M solutions, whereas part d represents a *13-nL* injection of a 6×10^{-12} M solution. The limit of detection (LOD) for a 4-nL injection is 3×10^{-12} M, or 12 zmol, calculated by using two times the peak-to-peak base-line noise. The peak in Figure 8c represents approximately 14 000 FITC molecules. Increasing the injection to 13 nL does not improve the mass detection limit but improves the LOD concentration to 1×10^{-12} M while retaining good efficiency.

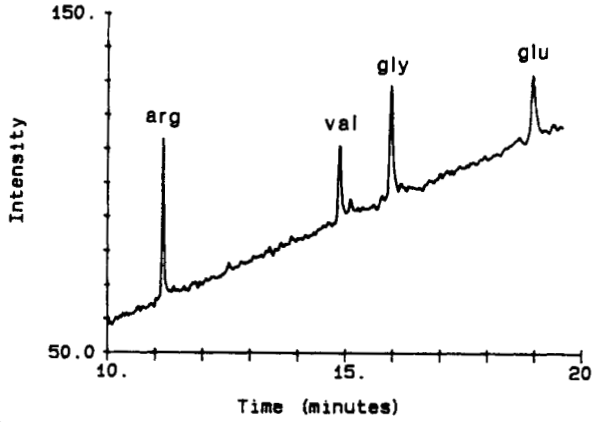

Figure 9. TDI electropherogram of four FITC–amino acids, with the concentration of injected FITC–arginine, FITC–valine, and FITC–glycine at 7×10^{-11} M and FITC–glutamate at 8×10^{-11} M. The fluorescence intensity is obtained by using a spectral window between the Rayleigh and major Raman band. The sloping base line is caused by a continually increasing integration time corresponding to a decreasing shift rate.

Figure 9 shows an electropherogram of four FITC–amino acids: arginine, valine, and glycine at 7×10^{-11} M, and glutamate at 8×10^{-11} M. The injection volume is 13 nL. The LODs for the FITC–amino acids are in the 20–80 zmol range, which compares favorably to the best previous work. Moreover, further improvements in the optical system, faster imaging spectrographs, optimized fluorophores, and optimized separation conditions are expected to push the sensitivity into the high yoctomole range in the near future.

ACKNOWLEDGMENT

We gratefully acknowledge the helpful advice and assistance of Stephen L. Pentoney, Jr., Xiaohua Huang, and Manny J. Gordon.

LITERATURE CITED

(1) Olefirowicz, T. M.; Ewing, A. G. *Anal. Chem.* **1990**, *62*, 1872–1876.
(2) Wallingford, R. A.; Ewing, A. G. *Anal. Chem.* **1988**, *60*, 1972–1975.
(3) Chien, J. B.; Wallingford, R. A.; Ewing, A. G. *J. Neurochem.* **1990**, *54*, 633–638.
(4) Kennedy, R. T.; Oates, M. D.; Cooper, B. R.; Nickerson, B.; Jorgenson, J. W. *Science* **1989**, *246*, 57–63.
(5) Jorgenson, J. W.; Lukacs, K. D. *Science* **1983**, *222*, 266–272.
(6) Gordon, M. J.; Huang, X.; Pentoney, S. L., Jr.; Zare, R. N. *Science* **1988**, *242*, 224–228.
(7) Ewing, A. G.; Wallingford, R. A.; Oleferowicz, T. M. *Anal. Chem.* **1989**, *61*, 292A–303A.
(8) Karger, B. L.; Cohen, A. S.; Guttman, A. *J. Chromatogr.* **1989**, *480*, 35–67.
(9) Roach, M.; Gozel, P.; Zare, R. N. *J. Chromatogr.* **1988**, *426*, 129–140.
(10) Nickerson, B.; Jorgenson, J. W. *HRC&CC, J. High Resolut. Chromatogr., Chromatogr. Commun.* **1988**, *11*, 533–534.
(11) Drossman, H.; Luckey, J. A.; Kastichka, A. J.; D'Cunhan, J.; Smith, L. M. *Anal. Chem.* **1990**, *62*, 900–903.
(12) Kuhr, W. G.; Yeung, E. S. *Anal. Chem.* **1988**, *60*, 2642–2646.
(13) Cheng, Y.-F.; Dovichi, N. J. *Science* **1988**, *242*, 562–564.
(14) Wu, S.; Dovichi, N. J. *J. Chromatogr.* **1989**, *480*, 141–155.
(15) Dovichi, N. J.; Cheng, Y.-F. *Am. Biotechnol. Lab.* **1989**, *7*, 10–14.
(16) Sweedler, J. V.; Bilhorn, R. B.; Epperson, P. M.; Sims, G. R.; Denton, M. B. *Anal. Chem.* **1988**, *60*, 282A–291A.
(17) Epperson, P. M.; Sweedler, J. V.; Bilhorn, R. B.; Sims, G. R.; Denton, G. R. *Anal. Chem.* **1988**, *60*, 327A–335A.
(18) Epperson, P. M.; Denton, M. B. *Anal. Chem.* **1989**, *61*, 1513–1519.
(19) Epperson, P. M.; Jalkian, R. D.; Denton, M. B. *Anal. Chem.* **1989**, *61*, 282–285.
(20) Koyashi, S.; Veda, T.; Kikumoto, M. *J. Chromatogr.* **1989**, *480*, 179–184.
(21) Brownlee, R. G.; Compton, S. W. *Am. Lab.* (*Fairfield, Conn.*) **1988**, *20*, 10–17.
(22) Cheng, Y.-F.; Piccard, R. D.; VoDinh, T. *Appl. Spectrosc.* **1990**, *44*, 755–765.
(23) Appendix E, Photometric Ltd. CC200 Operating Manual, Photometrics Ltd., 1989, Tucson, AZ.
(24) Huang, X.; Coleman, W. F.; Zare, R. N. *J. Chromatogr.* **1989**, *480*, 95–110.
(25) Huang, X.; Zare, R. N. *Anal. Chem.* **1990**, *62*, 443–446.
(26) Wallingford, R. A.; Ewing, A. G. *Anal. Chem.* **1987**, *59*, 1762–1766.
(27) Xi, X.; Yeung, E. S. *Anal. Chem.* **1990**, *62*, 1580–1585.
(28) Lei, W.; Fujiwara, K.; Fuwa, K. *Anal. Chem.* **1983**, *55*, 951–955.
(29) Mathies, R. A.; Peck, K.; Stryer, L. *Anal. Chem.* **1990**, *62*, 1786–1791.
(30) Jalkian, R. D.; Pomeroy, R. S.; Kolczynski, J. D.; Denton, M. B.; Lerner, J. M.; Grayzel, R. *Am. Lab.* (*Fairfield, Conn.*) **1989**, *21*, 80–88.
(31) Kolczynski, J. D.; Pomeroy, R. S.; Jalkian, R. D.; Denton, M. B. *Appl. Spectrosc.* **1989**, *43*, 887–891.
(32) Bredthauer, R. A.; Chandler, C. E.; Janesick, J. R.; McCurnin, I. W.; Sims, G. R. In *Instrumentation for Ground-Based Optical Astronomy*; Robinson, L. B., Ed.; Springer-Verlag: New York, 1987; p 468.
(33) Pemberton, J. E.; Sobocinski, R. L.; Sims, G. R. *Appl. Spectrosc.* **1990**, *44*, 328–330.
(34) Blackman, R. B.; Tukey, J. W. In *The Measurement of Power Spectra*; Dover: New York, 1958.
(35) Gassmann, E.; Kuo, J. E.; Zare, R. N. *Science* **1985**, *230*, 813–814.
(36) Pentoney, S. L., Jr.; Huang, X.; Burgi, D. S.; Zare, R. N. *Anal. Chem.* **1988**, *60*, 2625–2629.
(37) Huang, X.; Pang, T.-K.; Gordon, M. J.; Zare, R. N. *Anal. Chem.* **1987**, *59*, 2747–2749.
(38) Huang, X.; Gordon, M. J.; Zare, R. N. *Anal. Chem.* **1988**, *60*, 1837–1838.
(39) Huang, X.; Gordon, M. J.; Zare, R. N. *Anal. Chem.* **1988**, *60*, 375–377.
(40) Kawauchi, H.; Tuzimura, K.; Maeda, H.; Ishida, N. *J. Biochem.* **1969**, *66*, 783–789.
(41) Prober, J. M.; Trainor, G. L.; Dam, R. J.; Hobbs, F. W.; Robertson, C. R.; Zagursky, R. J.; Couzza, A. J.; Jensen, M. A.; Baumeister, K. *Science* **1987**, *238*, 336.

RECEIVED for review September 24, 1990. Accepted November 30, 1990. J.V.S. thanks the National Science Foundation for a postdoctoral fellowship administered under NSF Grant CHE-8907446. J.B.S. is a Howard Hughes Medical Institute Predoctoral Fellow. The support of Beckman Instruments, Inc., and of the National Institute of Mental Health under Grant No. MH45423 is gratefully acknowledged.